Multi Variant Surface Mounted Metal–Organic Frameworks

ARTICLE *in* ADVANCED FUNCTIONAL MATERIALS · AUGUST 2013

Impact Factor: 11.81 · DOI: 10.1002/adfm.201202996

4 AUTHORS, INCLUDING:

Bo Liu
University of Liverpool
17 PUBLICATIONS **1,360** CITATIONS
SEE PROFILE

Min Tu
Ruhr-Universität Bochum
15 PUBLICATIONS **117** CITATIONS
SEE PROFILE

ADVANCED FUNCTIONAL MATERIALS
www.afm-journal.de

www.MaterialsViews.com

Multi Variant Surface Mounted Metal–Organic Frameworks

*Bo Liu, Min Tu, Denise Zacher, and Roland A. Fischer**

Hybrid surface mounted metal–organic frameworks (h-SURMOFs) of multi variant core-shell (cs) and core–shell–shell (css) structures (SURMOF A-B and A-B-C, A: $[Cu_2(bdc)_2(dabco)]$; B: $[Cu_2(NH_2\text{-}bdc)_2(dabco)]$; C: $[Cu_2(ndc)_2(dabco)]$, bdc = 1,4-benzenedicarboxylate; NH_2-bdc = 2-amino-1,4-benzenedicarboxylate; ndc = 1,4-naphtalenedicarboxylate; dabco = 1,4-diazabicyclo[2.2.2]octane) with specific crystallographic [001] orientation and incorporated amino groups at a controllable depth within the bulk are deposited via liquid phase epitaxial (LPE) approach on pyridyl-terminated self-assembled monolayers (SAM). The location of the (amino) functionality can be precisely controlled through tuning the thickness (number of deposition cycles) of each sub-multilayer block according to the LPE deposition protocol. The chemo-selective and location-specific post deposition (chemical) modification of the amino groups in the cs and css-type h-SURMOF samples is achieved. The h-SURMOFs allow one to probe functional groups at certain location in the volume of hybrid MOF crystallites attached to surfaces as thin film coatings. Multiplex adsorption kinetics of FPI (FPI = 4-fluorophenyl isothiocyanate) is observed in h-SURMOFs due to their multi-variant pore structures in samples of A-B and A-B-C. Conceptually, the stepwise LPE growth method enables fabrication of hybrid SURMOFs and incorporation of multi-variant functionalities into one homogeneous thin film material, providing precisely tunable pore environment for selective adsorption, separation, etc.

1. Introduction

Metal–organic frameworks (MOFs; including porous coordination polymers, PCPs) are built from inorganic coordination units and organic ligands, where the ligands act as "struts" that bridge the metal coordination units which in turn act as 'joints' in the resulting MOF architecture. The structural diversity, high porosity, and thermal stability make MOFs ideal candidates for a wide range of applications like gas storage and separation, selective heterogeneous catalysis, carbon dioxide capture, guest dependent luminescence, etc.[1] Precise control of the physical and/or chemical properties of MOFs such as pore size/shape, composition etc, has been an ongoing challenge for optimizing their functions.[2] Pore structures (size, shape, etc.) and coordination space in MOFs are crucial factors to influence their performances, which can be tailored/tuned via specific ligand design and post synthetic modification (PSM).[3]

A large group of MOFs mainly involve single organic linkers, including most representative MOFs, such as IRMOFs,[4] ZIFs,[5] etc, in which organic linkers adopted the same configuration in resulting frameworks and lead to the unitary pore structure and environment. However, MOFs comprised of two or more organic ligands (or linkers) emerged and became increasingly prevalent.[6] In a typical class of jungle-gym structured compounds of the general formula $[M_2L_2P]$ (M = Cu^{2+}, Zn^{2+} Co^{2+}, Ni^{2+}; L = dicarboxylate, P = dinitrogen pillar ligand), di-anionic dicarboxylate linkers connect M_2 units in a paddle-wheel fashion into 2D layers and neutral N-based pillar linkers bridge the layers into a 3D network, where two linkers play different structural roles.[6a,7] Another strategy is involving auxiliary ligands to construct MOF networks in which these auxiliary ligands are used for forming metal coordination units, namely, secondary building units (SBUs), but do not directly anticipate in the formation of frameworks.[8] This strategy is especially useful to design chiral MOFs involving chiral coordination units comprised of auxiliary ligand.[9] In some case, solvent molecules also play this role, e.g., H_2O in HUKST-1[10] and MILs.[11] These "traditional" MOFs are herein considered as having single-functionality due to their uniform composition (i.e., regular, crystalline order of chemical functionality), unitary pore structure and environment.

In contrast, rapid growing research interests are being paid on the multi-functional MOFs, which are regarded as single phase MOF materials (rather than a mixture) having multivariate functionalities and multiplex pore structures and environments.[12] Mixed component MOFs (MC-MOFs),[12a] MIXMOFs,[12b] multivariate MOFs (MTV-MOFs),[12c] which are comprised of various linkers, however with the same structural role, have been developed and displayed the properties that are not simply the linear combinations of those of the parent MOFs. Remarkably, eight different dicarboxylates could be incorporated into a single MTV-MOF with tunable degree of incorporation of the different ligands. And they showed the effect "whole is better than the sum of its parts" as evidenced by their fourfold enhancement of gas adsorption and separation properties in comparison with their simple single link analogs.[12c] In addition, macro-scale **BAB**-type heterocrystals of MOFs (or PCPs)[13] and core-shell MOFs[14] have been

Dr. B. Liu, M. Tu, Dr. D. Zacher, Prof. R. A. Fischer
Chair of Inorganic Chemistry II–Organometallics and Materials Chemistry
Ruhr-Universität Bochum
D-44780 Bochum, Germany
E-mail: roland.fischer@rub.de

DOI: 10.1002/adfm.201202996

reported and were fabricated via solvothermal, heteroepitaxial growth. These efforts are devoted to incorporate multi-variant functionality into MOFs by using multiple linkers and at the same time keeping the framework topology (crystal structure) invariant. This concept offers a new dimension of controlling pore sizes, pore gates, distribution of chemical function and over-all compositions, and hence allows tailoring properties of MOFs beyond the limits of mono-functional MOFs.

The above sketched progress mainly deals with bulk MOFs as single crystals or microcrystalline powder samples, typically synthesized using solvothermal syntheses. The essential limitation of this approach relies with the lack of the precise control the location/distribution of functionalities in the volume of the MOF crystallites (particles), where their random location/distribution is probably dominated by the energy of functional group interactions and steric interactions, etc.[12a,c,i] Also, it turned out to be difficult to control (or predict) the linker ratio in a resultant bulk multi-functional MOF material. This is directly related to the limitation of the one-pot solvothermal synthetic approach in which reaction process occurs in a sealed vessel like a "black box" and cannot be easily intervened.[15] Recently introduced step-by-step liquid phase epitaxial (LPE) approach for the fabrication of surface attached MOF crystallites forming thin films (SURMOFs) (Supporting Information) is exactly aligned to these challenges.[16] In a step-by-step liquid phase epitaxial process, sequential deposition of inorganic and organic building blocks onto the functionalized substrate allows the precise control the location/distribution and thickness/amount of the functionalities in thin film bulk, depending on the deposition sequence and cycles of different components. Ideally, the growth mode of SURMOF thin films is expected to have a resolution of "one unit cell/layer" and it is proportional to the number of LPE deposition cycles.[16,17] Stepwise LPE has shown its power for deposition of MOF (hetero-/hybrid-)structures,[18] for suppressing interpenetration[19] and for tailoring the chemical functionality of the external SURMOF surface (i.e., the topmost layer),[20] etc. Using LPE, preparation of the hybrid SURMOFs by depositing MOF-**B** on the seeding layers of MOF-**A** on functionalized substrate have been demonstrated, for example $[Zn_2(ndc)_2(dabco)]$-on-$[Cu_2(ndc)_2(dabco)]$,[18a] $[Cu_2(F_4bdc)_2(dabco)]$-on-$[Cu_2(ndc)_2(dabco)]$ and $[Zn_2(BME\text{-}bdc)_2(dabco)]$-on-$[Cu_2(ndc)_2(dabco)]$,[18b] based on the lattice match between two MOFs. Nevertheless, only structures and characterizations were reported and no reactive functional groups were incorporated into these hybrid SURMOFs (h-SURMOFs).

In this work, we addressed above challenges via the preparation, characterization and chemo-selective and location-specific post deposition chemical modification (PDM) of functional ($-NH_2$) multilayers in hybrid SURMOFs positioned as top block and as block multilayers at a defined deeper position as well. We introduce PDM as a synonymous technical term with respect to post synthetic modification (PSM) but highlighting SURMOFs as the object of chemical modification. On one side, the location/distribution and ratio of functionalities are precisely controllable, in contrast to their random distribution in crystal/bulk powder MOFs. On the other hand, hybrid binary $[Cu_2(NH_2\text{-}bdc)_2(dabco)]$ (**B**) on $[Cu_2(bdc)_2(dabco)]$ (**A**) and ternary SURMOF $[Cu_2(ndc)_2(dabco)]$ (**C**) on $[Cu_2(NH_2\text{-}bdc)_2(dabco)]$ (**B**) on $[Cu_2(ndc)_2(dabco)]$ (**A**) contain both inert (**A** and **C**) and active multilayers (**B**) (NH_2-bdc = 2-amino-1,4-benzenedicarboxylate; bdc = 1,4-benzenedicarboxylate; ndc = 1,4-naphtalenedicarboxylate; dabco = 1,4-diazabicyclo[2.2.2]octane). The use of NH_2-bdc allowed selective post-synthetic modification by 4-fluorophenyl isothiocyanate (FPI), as our choice of a probe molecule, via chemical binding and formation of thiourea linkages. Importantly, h-SURMOFs exhibit multiplex adsorption kinetics of guest molecules which implies a multi-variant pore structure.

2. Result and Discussion

Heteroepitaxial growth of one porous material on surface of another requires lattice matching at the interface.[21,22] Core/shell structured and **A**-**B**-**A** type block hybridized MOFs can be prepared depending on the choice of MOF candidates. In a heterometallic core/shell structure of $[M_2L_2P]$ type MOFs (tetragonal) $[Zn_2(ndc)_2(dabco)]$(core)/$[Cu_2(ndc)_2(dabco)]$ (shell),[13] surface terminated carboxylate on [100] and [010] faces and nitrogen pillar ligands on [00l] were used as coordination sites for growth of isostructural shell crystal of $[Cu_2(ndc)_2(dabco)]$. In contrast, face-selective epitaxial growth in the system of $[Zn_2(ndc)_2(dabco)]$/$[Zn_2(ndc)_2(dpndi)]$ (dpndi = N,N-di(4-pyridyl)-1,4,5,8-naphthalenetetracarboxydiimide),[14a] leads to the **ABA** type block porous coordination polymers. Likewise, IRMOF-**1** and IRMOF-**3** hold the same cell parameters and hence sequential growth on the seeding crystals generate core-shell structure due to the lattice matching in all crystallographic faces.[14b,c] In addition, heteroepitaxial growth is also well suited for preparation of multifunctional zeolite films and membranes with controlled microstructure.[22]

The various types of hybrid bulk MOF structures can be transferred onto a surface by step-by-step liquid phase epitaxial (LPE) approach. LPE provides the unique advantage to fabricate surface mounted MOFs as thin films (SURMOFs) with controllable orientation and thickness of the crystallites or crystalline domains with respect to the underlying substrate. It is very well confirmed that after nucleation and orientation of the initial SURMOF crystallites is established on a growth directing SAM modified substrate, subsequent deposition of the same MOF results in growth along the same crystallographic orientation due to the seeding/templating effect.[16,23] Heteroepitaxial growth may occur in case of another MOF with suited lattice match in the particular growth direction.[18] The very well established fundamentals for preparation of hybrid MOFs in both bulk and thin film level enables us to largely design hetero-structured MOFs for tailored properties and applications. Layer-based tetragonal MOFs exhibit a general formula $[M_2L_2P]$ (M: Cu^{2+}, Zn^{2+} Co^{2+}, Ni^{2+}; L: dicarboxylate linker; P: dinitrogen pillar ligand),[6a,7] and consist of 2D layers of [ML] which can be connected into 3D network structures by dinitrogen pillar ligand as stated above. These compounds have been well investigated for SURMOF growth via stepwise LPE method.[18,23] One can consider bdc and dabco as parent ligand L and pillar P respectively. Various derivatives of L and P are possible such as such as F_4bdc, ndc, NH_2-bdc etc. and 4,4´-bipyridine etc. The L and P and their derivatives adopt the same structural role;

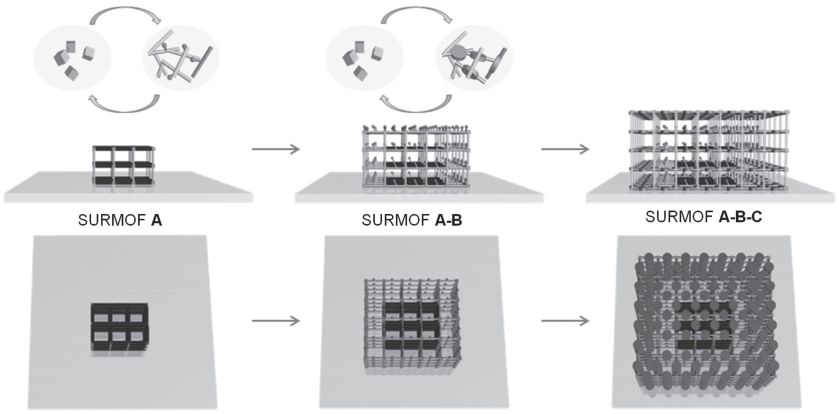

Figure 1. Schematic illustration of hybrid SURMOF growth by starting from SURMOF $[Cu_2(bdc)_2(dabco)]$ (A) on PPMT SAM on gold substrate, which is prepared by alternating deposition of $Cu(Ac)_2$ and equimolar mixture of bdc/dabco ethanol solution, separated by washing step with pure ethanol (Supporting Information Figure S1). Subsequent growth of multilayers $[Cu_2(NH_2\text{-}bdc)_2(dabco)]$ (B) on A using NH_2-bdc instead of bdc gives rise to the formation of core-shell hybrid SURMOF A-B. Replacing NH_2-bdc with ndc, and growth of another multilayers $[Cu_2(ndc)_2(dabco)]$ (C) lead to core-shell-shell structure A-B-C. The thicknesses of each block of layers are tunable by the number of deposition cycles. The SURMOFs A, A-B and A-B-C are depicted as front view (above: [100]-face terminated by carboxylic acid linkers) and top view (below: [001]-face, terminated by dabco ligands).

however, they greatly alter the pore structures and the chemical environments of the coordination space in the resultant MOFs (and SURMOFs) and influence their properties accordingly. In the following, we illustrate our strategy using $[M_2L_2P]$ type layer-based MOFs as model to integrate multi-functionality at varied positions (multilayer block on top or within the bulk) of the hybrid SURMOFs as displayed in **Figure 1**.

2.1. Preparation and Characterization of SURMOFs A, A-B and A-B-C

SURMOF **A** of $[Cu_2(bdc)_2(dabco)]$ oriented in [001] direction on PPMT SAMs was prepared following the typical procedure described in our previous work (Supporting Information Figure S1).[18,23] Sequential depositions of $[Cu_2(NH_2\text{-}bdc)_2(dabco)]$ (**B**) and $[Cu_2(ndc)_2(dabco)]$ (**C**) adopted the same growth parameter with that for $[Cu_2(bdc)_2(dabco)]$. The terminal step for SURMOF **A** growth is the deposition of bdc/dabco that leaves carboxylate groups and dabco groups in [100]/[010] and [001] direction, respectively. These surface-exposed functional groups provided similar templating effect as functional terminal groups of SAMs do, for subsequent growth of multilayers of $[Cu_2(NH_2\text{-}bdc)_2(dabco)]$ (**B**). Similarly, $[Cu_2(ndc)_2(dabco)]$ (**C**) can be deposited on top of **B**. It should be noted that **A**, **B**, and **C** are isostructural and have the same cell parameters (Supporting Information Figure S2). As discussed above, the heteroepitaxial growth rests on this lattice matching at the interface among **A**, **B**, and **C**. In [001] direction, all three MOFs are comprised of the same coordination units of Cu-dabco, hence this allowed sequential growth in this direction. In [100]/[010] directions, they contain Cu-bdc, Cu-NH_2-bdc and Cu-ndc in **A**, **B**, and **C**, respectively, however, the coordination modes are the same in the three blocks. Therefore, the growth of hybrid SURMOFs occurred not only perpendicular ([001] direction) but also parallel ([100]/[010] directions) to the surface (Figure 1) and it is rational to expect a core-shell and core-shell-shell hybrid structure for SURMOF **A-B** and **A-B-C**, respectively, which are confirmed by XRD and SEM data as discussed below.

The growth of hybrid SURMOF is in situ monitored by quartz crystal microbalance (QCM) as displayed in **Figure 2**. The QCM profile demonstrates a continuous mass uptake for the growth of SURMOF **A** (10 cycles) on PPMT SAM polished QCM substrate (Figure 2a). Continuous and sequential deposition of **A** (10 cycles) and **B** (10 cycles) gave rise an approximately linear growth (Figure 2b). Similarly, multilayers **C** can be deposited on top of **B** on **A** (Figure 2c) as depicted in Figure 1. This implies the successful fabrication of hybrid SURMOF samples. Our QCM data is in accordance with the independent experiments for depositions of **A**, **B**, and **C** on PPMT SAM functionalized gold substrates.[18,20,24] Since the initial cycles of deposition are responsible for the nucleation, it is reasonable to have a fast growth. SURMOF **A** first nucleated on the surface and then was used as seeding nuclei for subsequent growth of **B** and **C**, thus displayed a somehow larger mass uptake in each step for the deposition of **A** in comparison with

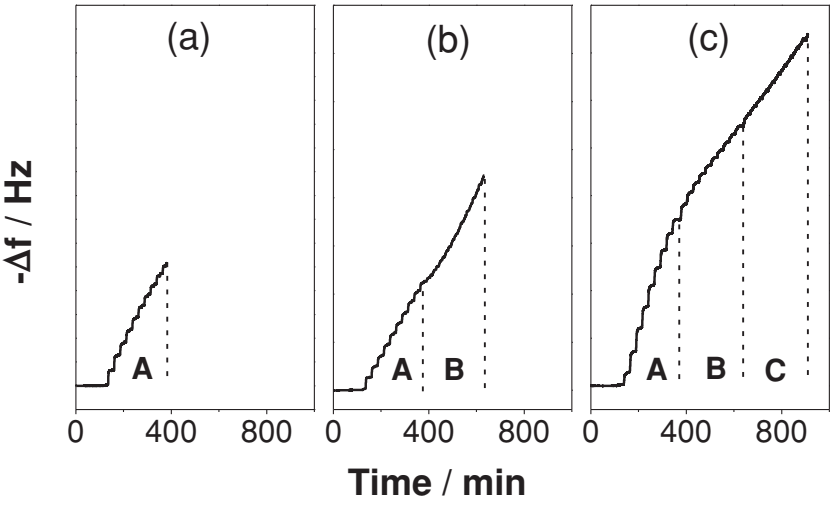

Figure 2. In situ QCM monitoring of typical SURMOF growth (number of cycles in parentheses): a) SURMOF A(10), b) SURMOF A(10)-B(10) and c) SURMOF A(10)-B(10)-C(10) on PPMT SAM modified gold coated QCM substrate. All depositions adopted the same parameters. Similar samples with variation of the number of growth cycles were obtained.

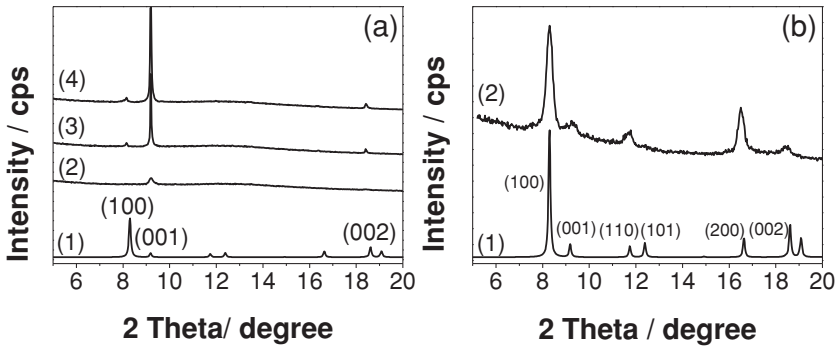

Figure 3. a) Out-of-plane XRD patterns: (1) simulated pattern of bulk A; (2) SURMOF A(15); (3) SURMOF A(15)-B(15) and (4) SURMOF A(15)-B(15)-C(15) and b) in-plane XRD patterns: (1) simulated pattern of bulk A and (2) SURMOF A(15)-B(15)-C(15).

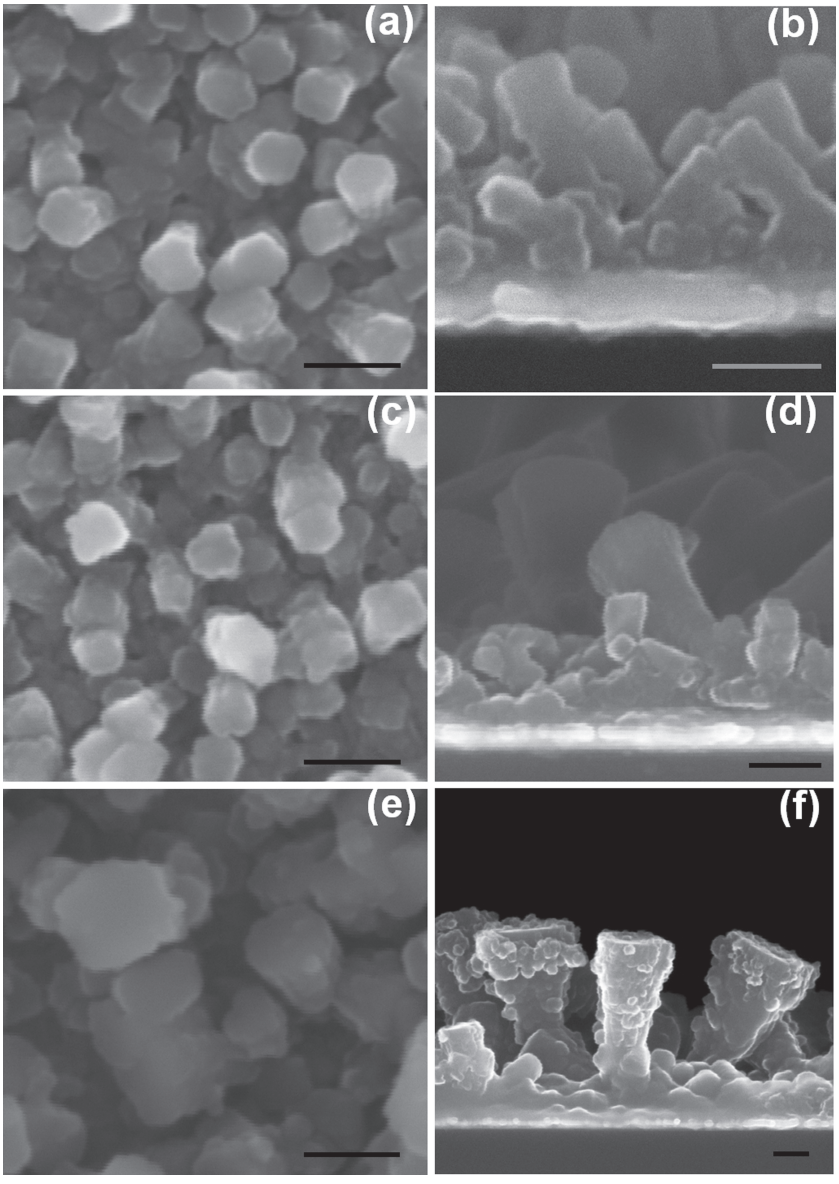

Figure 4. SEM images of SURMOF A(20) a) topography and b) cross-section; A(20)-B(20): c) topography and d) cross-section and A(20)-B(20)-C(20): e) topography and f) cross-section. All scale bars: 200 nm.

that of **B** and **C**. This is in agreement with the crystallite size and morphology evolution as observed by SEM (see below). It has been well studied that PPMT SAM is favorable for [001] orientation growth of layer-based MOFs ($[M_2L_2P]_n$).[16,18b] As examined by surface X-ray diffraction in and out of plane mode, SURMOF **A** (15 cycles) showed one single peak around 9.20° (2θ), indicating a [001] orientation growth according to the XRD data simulated from powder sample (**Figure 3**a and Supporting Information Figure S3). The deposition of 15 cycles of **B** on **A** gave rise to the intensity increase of [001] peak and the intensity kept increasing after another 15 cycles of **C** was deposited. It suggested successful fabrication of crystalline **C**-on-**B**-on-**A** on the SAM template surface. The correlation of the [001] peak intensities calculated from integrated areas against the numbers of deposition cycles reveals an approximately linear growth mode (Supporting Information Figure S3 (insert) and Table S1), matching the QCM data. Out-of-plane XRD measurements are carried out independently on another three series of samples with varied deposition cycles in each sub-layers (Supporting Information Figure S4), which indicated similar results and confirmed the reproducibility. In-plane XRD pattern of SURMOF **A-B-C** matches well with the simulated one from powder XRD data (Figure 3b). Note that deposition of **B** on **A** led to the appearance of [100] peak of low intensity and subsequent **C** growth slightly increased this peak (Figure 3a). This agreed with the weak [001] peak for SURMOF **A-B-C** in the in-plane XRD pattern, because in-plane XRD is sensitive to those lattice planes parallel to substrate, whereas out-of-plane XRD detects the lattice planes perpendicular to substrate. Nevertheless, the final SURMOF samples **A**, **A-B** and **A-B-C** were still highly oriented in [001] direction due to very low intensity of [100] peak.

Topographic and cross-sectional morphologies of the prepared SURMOF samples are observed by scanning electronic microscopy (SEM) as shown in **Figure 4** (high magnification) and Supporting Information Figure S5 (low magnification). The images of theses samples reveal homogeneous thin films comprised of densely stacked crystallites and sizes of crystallites are well-distributed. This is consistent with the morphologies of SURMOF $[Cu_2(ndc)_2(dabco)]$ as we observed previously.[20] Inverted cone-like crystallites were found to stand erect on the substrate surface, which corresponds to the preferred growth direction of SURMOF on the SAM

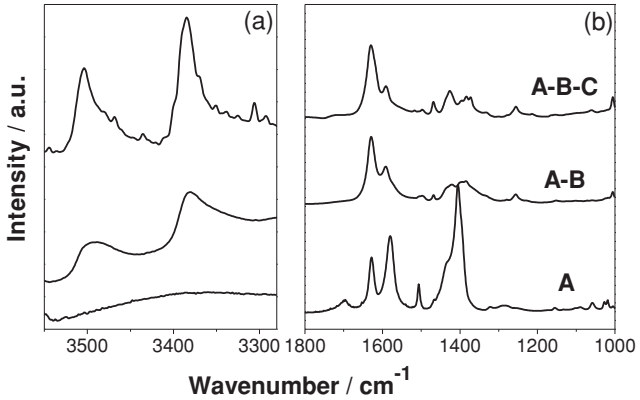

Figure 5. IRRA Spectra for SURMOF A, A-B and A-B-C on gold substrate: a) between 3520 and 3280 cm^{-1} for N-H vibrations and b) from 1800 to 1000 cm^{-1} for vibrations of MOF skeletons.

template. The increasing sizes of crystallites in three dimensional directions with sequential deposition of **A**, **B**, and **C** were observed from both topographic and cross-sectional view. This is in agreement with XRD intensities increase of [001] diffraction peak and shows us the direct proof of the heteroepitaxial growth as schemed in Figure 1. It is noteworthy that the size of crystallites (100–200 nm) observed in Figure 4 by SEM is much larger than those anticipated by a layer-by-layer growth, typically 1 nm for 1 cycles in case of $[Cu_2(ndc)_2(dabco)]$.[18b] SEM images of high magnification of SURMOF **A-B-C** (Supporting Information Figure S6) revealed that large crystallites are comprised of smaller particles which size may be in line with a layer-by-layer, self-limiting growth fashion. Nevertheless, total mass deposition by QCM is approximately a linear function of the number of cycles (Figure 2).

IRRAS (Infrared Reflection Absorption Spectra) for SURMOF **A**, **A-B**, and **A-B-C** on PPMT SAM modified gold substrate were recorded. In comparison with IRRAS of SURMOF **A**, SURMOF **A-B** and **A-B-C** displayed the typical N-H vibrations around 3500 and 3380 cm^{-1} (**Figure 5**), implying the incorporation of amino groups. It is worth to note that the deposition sequence can not be changed freely in this particular system, unfortunately. Our trial to prepare SURMOF **A**-on-**B**-on-**A** was unsuccessful, as evidenced by XRD. It is assumed that the coordination equilibrium of the different ligands with Cu^{2+} is responsible for this phenomenon at the conditions of the LPE. The deposition sequence is vital for the fabrication of hybrid SURMOFs of the type discussed herein. One should be aware of hybrid **A**-**B**-**A** being a heterostructural macrocrystal in nature of crystal of **A**-on-**B** from two sides.[13]

In principle, following our stepwise LPE concept, a multivariant functionality can be integrated in the hybrid SURMOFs depending on the selected parent MOFs. In this work, we incorporated functional groups ($-NH_2$) in order to demonstrate the power of the concept. They can be deposited on the top (multi-) layers (SURMOF **A**-**B**) or embodied at a given position deeper in the hybrid crystallites of the film (SURMOF **A**-**B**-**C**). Essentially, the thickness of each sub-block of multilayers can be precisely controlled by adjusting their deposition cycles (Supporting Information Figure S4). That means that the location/position of the incorporated functionalities is tunable. In contrast, the location of functionalities in conventional bulk MTV-MOFs or related mixed component MOFs is less clear. The incorporation of different ligands eventually creates multiplex pore structures and environments in resultant hybrid SURMOFs, as discussed following.

2.2. Post Deposition Modification of Hybrid SURMOFs and QCM Gas Adsorption Studies

The installed amino groups in both h-SURMOF **A-B** and h-SURMOF **A-B-C** should allow post-synthetic modification by 4-fluorophenyl isothiocyanate (FPI), because amino groups can react with isothiocyanate under mild condition and form the robust thiourea bond.[25] Meanwhile, FPI can be physisorbed in the accessible pore space in the h-SURMOFs. XPS data (monitoring the F 1s signal) demonstrated that FPI physically adsorbed in SURMOF **A** can be completely removed by vacuum treatment (**Figure 6**). However, FPI adsorbed in

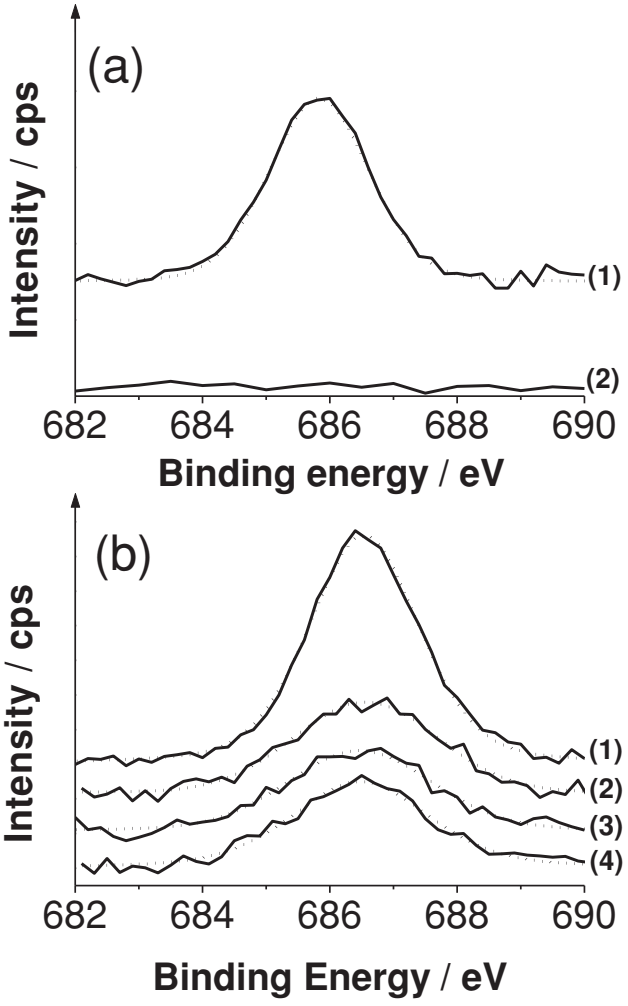

Figure 6. F 1s XPS spectra (dotted line: fitted; solid line: measured) of a) SURMOF A(30): (1) FPI-loaded and (2) treated in vacuum for 30 min and b) SURMOF A(10)-B(10): (1) FPI-loaded, (2) treated in vacuum for 30 min, (3) heated in vacuum at 40 and (4) 54 °C.

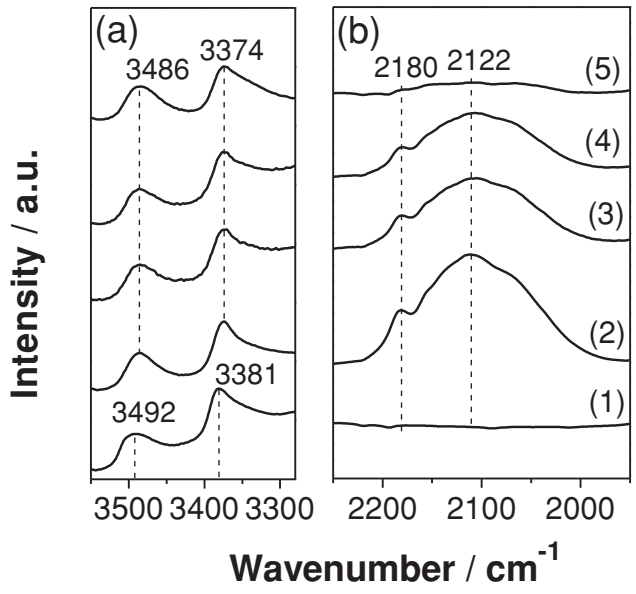

Figure 7. IRRAS spectra for SURMOF A-B: (1) as-prepared, (2) FPI loaded and vacuum treated for (3) 1 h, (4) 2h and (5) overnight: a) between 3520 and 3280 cm^{-1} for N-H vibrations and b) characteristic vibration region for isothiocyanate (NCS) group.

h-SURMOF **A-B** cannot be removed completely. Even after prolonged heating up to 54 °C in vacuum a significant residual F 1s signal remained. This feature is assigned to the formation of a robust thiourea covalent linkage between amino groups and FPI. The co-existence of physical and chemical adsorption of FPI has been also approved by IRRAS studies (**Figure 7**). h-SURMOF **A-B** was firstly evacuated overnight to remove the solvent (ethanol) inside of pores and then exposed to the naturally generated FPI vapor overnight for FPI loading. In comparison with IRRAS of the as-prepared sample, a new broad band centered at 2122 cm^{-1} with a shoulder band around 2180 cm^{-1} appears in FPI loaded sample. This broad band is assigned to the vibration of NCS band according to the experimental spectra and theoretical calculations reported by Szaleniec et al.[26] and hence conform the successful FPI loading in h-SURMOF **A-B**. However, other bands from FPI can not be observed due to their low intensity and overlap with MOF skeletons and vibrations of MOF skeletons kept intact during FPI adsorption-desorption process (Supporting Information Figure S7). Shifts of N-H vibrations from 3492 and 3381 to 3486 and 3374 cm^{-1}, respectively, were observed, implying the reaction between amino and isothiocyanate groups. These IR shifts are consistent with FPI post-synthetic modification of h-SURMOF of $[Cu_2(NH_2\text{-bdc})_2(dabco)]$ reported very recently.[24b] Intensity of NCS vibrations was decreased with evacuation and almost completely vanished after vacuum treatment overnight. This is assigned to desorption of physically adsorbed FPI. In contrast, N-H vibrations remaining nearly invariable approved the robustness of thiourea bond. Furthermore, adsorption and post-synthetic modification of FPI were performed on microcrystalline powder samples of $[Cu_2(bdc)_2(dabco)]$ and $[Cu_2(NH_2\text{-bdc})_2(dabco)]$. IR studies (Supporting Information Figure S8 and S9) displayed a similar result in comparison with those of SURMOF samples and further favored co-existence of FPI in hybrid SURMOFs as well as selective and specific modification. From these data and comparisons it is concluded that selective post deposition chemical modification (PDM) is achieved on top multi-layers (outer shell) of h-SURMOF **A-B** after removal of physically adsorbed, excess FPI. h-SURMOF **A-B-C** displayed similar behaviors with FPI loading and de-loading as confirmed by IRRAS spectra (Supporting Information Figure S10). In this latter case, PDM in the inner shell of the hybrid core-shell-shell structure was achieved since FPI can penetrate into the each sub-multilayer (Supporting Information Figure S11 and S12). One can specify the modification at a certain penetration depth by altering the thickness of each block (core and shells) of the hybrid crystallites.

It has been demonstrated that SURMOFs grown on QCM substrates allowed the monitoring of adsorption/desorption of guest molecules and enabled the determination of the corresponding diffusion constants under ideal circumstances.[27] In addition, we have shown enantioselective adsorption of chiral guest molecules over homochiral SURMOFs[28] and the outer surface functionalization of SURMOFs with a fluorescent probe molecule.[20] Accordingly, the FPI adsorption over SURMOF **A**, **A-B** and **A-B-C** was semi quantitatively analyzed using QCM (**Figure 8**). When the evacuated SURMOF A were exposed to FPI vapor using N_2 as carrier, the adsorption took place immediately and got to saturation very fast (Figure 8a). The control experiment of N_2/FPI (vapor) flows over bare gold

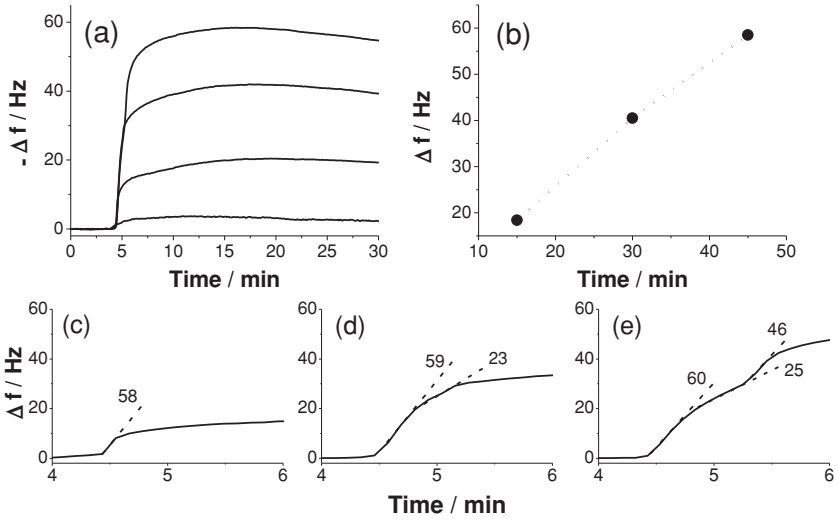

Figure 8. a) In situ QCM monitoring gas phase FPI (vapor) loading over evacuated SURMOF A, A-B and A-B-C (15 cycles for each sub-multilayer of A, B and C) using N_2 as carrier at a flow rate of 5 sccm; b) the plot of FPI adsorption against total sample deposition cycles (Supporting Information Table S2) and analysis of FPI adsorption kinetics (by slope, -df/dt in [Hz·s^{-1}]) on c) SURMOF A, d) SURMOF A-B and e) SURMOF A-B-C. The slope is evaluated by linear fitting of each linear part of the adsorption curve.

substrate gave rise to a negligible mass uptake. The saturated adsorption amount is approximately proportional to the total cycle numbers (i.e., the deposited SURMOF mass) for samples of **A**, **A-B** and **A-B-C** (Figure 8b and Supporting Information Table S2). SURMOF **A** (15) possessed unitary pore environment and thus exhibited a linear FPI (physical)adsorption (slope: 58 $Hz \cdot s^{-1}$) to saturation within ca. 8 s. SURMOF **A** (15)-**B** (15) took about 45 s to reach the saturation adsorption with a roughly two fold amount in comparison with SURMOF **A**. Two stage adsorptions were observed for h-SURMOF **A-B**, which is in accordance with physical and chemical adsorption of FPI in multilayers of **A** and **B**. The slope (59 $Hz \cdot s^{-1}$) of the first adsorption is very close to that in SURMOF **A** and the other much slower adsorption slope of 23 $Hz \cdot s^{-1}$ can be ascribed to the FPI adsorption in multilayers of **B** owing to the smaller pore space and reaction process between isothiocyanate and amino groups. It is noteworthy that the FPI sensing by QCM is an adsorption-dominated process in which mechanistic details on the atomistic level are difficult to elucidate quantitatively. Our interpretation of the QCM data is a qualitative one which is based on the following reasoning. The guest molecule diffusion in porous materials such as MOFs is fast, at a time scale of millisecond even at the temperatures lower than 240 K, as evidenced by ^{129}Xe 2D-exchange NMR spectroscopy (EXSY), however, the time resolution of QCM is low (second scale).[29] Therefore, it is rational to assume that the shell **B** firstly behave as passage for FPI molecules to penetrate through until FPI adsorption at the core **A** reached saturation. On the other hand, only those molecules which are coupled with QCM substrate by physio- or chemisorption mass uptake can be sensed by QCM. That means the molecules in free transportation in pores of MOFs can not be detected by QCM. On the whole, FPI loading takes place from outer blocks and then FPI diffuses into inner blocks; however, mass uptake sensing by QCM is effected and thus measured in an inverted fashion.

h-SURMOF **A-B-C** displayed a more complicate adsorption process and it took longer time (70 s) for saturation adsorption. Three steps of adsorption were associated with the triple-variant pore structures in h-SURMOF **A-B-C** as discussed above. Importantly, the first two steps of adsorption are very similar with that occurred in h-SURMOF **A-B**, matching our expectations deduced from the above discussed reasoning. The third step adsorption with a slope of 46 $Hz \cdot s^{-1}$ can be attributed to the adsorption in multilayers of $[Cu_2(ndc)_2(dabco)]$ of the outer shell. The uptake it is somewhat lower than that in multilayer of $[Cu_2(bdc)_2(dabco)]$ due to the smaller pores. It should be clarified that a very small window opening (ca. $2 \times 2Å^2$) of h-SURMOF **A-B-C** [001] plane is subject to ndc linker in outer shell **C** (Supporting Information Figure S11), which will prevent guest molecules from accessing in this direction. In contrast, the window opening (ca. $2 \times 7Å$) of the [100] plane is much larger and allows FPI (ca. 2.5×7.5 Å) to slide in. For **A** and **A-B**, the opening in both [100] and [001] planes are large enough for FPI to pass through. The uptake in multilayer of $[Cu_2(NH_2\text{-}bdc)_2(dabco)]$, i.e., the **B** part of the structure, is the lowest. This probably arises from the reaction between amino and isothiocyanate groups as discussed above. These interpretations of the QCM data match quite nicely with the hybrid core-shell-shell (css) structure of **C**-on-**B**-on-**A** and elucidate the multiplex characteristics in hybrid SURMOFs with respect to adsorption kinetics. Provided crystallites of **A**, **B**, and **C** were separately grown and distributed (like a simple mixture) on the substrate rather than formation of hybrid css-structures, the FPI adsorption should occur synchronously and only show the longest QCM response time among **A**, **B**, and **C**. The observed stepwise adsorption behaviors agree well with the heteroepitaxial growth scheme and the formation of the hybrid structures as indicated by XRD and SEM. Additionally, equilibrium adsorption isotherms of some other volatile organic compounds (methanol, acetonitrile, cyclohexane and FPI) as probe molecules were also examined on the h-SURMOF **A-B-C** as presented in Supporting Information Figure S12, which further confirmed that small guest molecules are able to freely enter the pores of **A-B-C**. The hybrid SURMOFs offer not only chemically inert and reactive pores but also three different pore environments as well as controllable location of the onset of the specific pore structure which contribute to the peculiar FPI uptake kinetics. This type of multi-variant and hence multifunctional SURMOFs provides us with novel opportunities to control the adsorption characteristics of the MOF thin film by the LPE deposition protocol. In particular, fine-tuning of the hybrid film structure can control the kinetics of guest molecule uptake. Importantly, a selective and location specific post deposition chemical modification can be achieved by using the SURMOF concept.

3. Conclusions

Hybrid SURMOFs $[Cu_2(NH_2\text{-}bdc)_2(dabco)]$(**B**)-on-$[Cu_2(bdc)_2(dabco)]$(**A**) and $[Cu_2(ndc)_2(dabco)]$ (**C**)-on-$[Cu_2(NH_2\text{-}bdc)_2(dabco)]$(**B**)-on-$[Cu_2(bdc)_2(dabco)]$(**A**) were prepared through stepwise liquid phase epitaxial approach and fully characterized by QCM, surface X-ray diffraction, IRRAS, XPS, and SEM. Functional (amino) group can be installed on top of or embodied into the hybrid SURMOF at a given position within the bulk of the SURMOF crystallites. Physical and chemical adsorption of guest molecule (FPI) co-existed in hybrid SURMOFs and chemo selective and location specific post deposition chemical modification can be achieved. The hybrid SURMOFs exhibited distinct adsorption kinetics of FPI due to the different pore environments within the core, core-shell and core-shell-shell structures of the SURMOF crystallites.

Stepwise LPE makes it facile to fabricate these more complicate structured MOF thin film materials by incorporating a pre-defined variety of functionalities and pore structures into one hybrid material. The hybrid SURMOF concept enables precise control of the amount and location/distribution of functionalities for tailored properties. h-SURMOFs with a defined, multi-variant sub-structure grown on QCM substrates as we described herein may serve as valuable devices to discriminate the adsorption behavior of analytes from mixtures according to their different adsorption kinetics. Such kind of multi-variant SURMOFs with even more sophisticated sub-structures are suggested to exhibit excellent potential for advanced separation tasks, for example as stationary phases for PLOT columns in capillary GC, especially for complicate mixtures[30] or for components in smart membranes.[31]

4. Experimental Section

Materials: Reagents and solvents were purchased from commercial sources and were used without further purification (2-amino-1,4-benzenedicarboxylate (99%), Aldrich; 1,4-benzenedicarboxylate (99%), Fluka Chemie; Copper(II) acetate monohydrate (98%), Fisher Chemical; 1,4-diazabicyclo[2.2.2]octane (95%), Fluka Chemie; 4-fluorophenyl isothiocyanate (98%), Aldrich; ethanol (absolute), Aldrich; 1,4-naphtalenedicarboxylate (94%), Aldrich).

Preparation of SURMOF $[Cu_2(bdc)_2(dabco)]$ (A), $[Cu_2(NH_2\text{-}bdc)_2(dabco)]$ (B), $[Cu_2(ndc)_2(dabco)]$ (C): The PPMT (PPMT = (4,(4-pyridyl)phenyl)-methanethiol) SAMs were fabricated following standard procedures using either 150 nm Au/2 nm Ti evaporated on Si wafers, or commercially available quartz crystal microbalance (QCM) Au substrates.[18] The components were applied as diluted ethanol solutions: Cu(II) acetate hydrate (0.5 mM), an equimolar mixture (0.2 mM) of bdc (bdc = 1,4-benzenedicarboxylate; A) and dabco (dabco = 1,4-diazabicyclo[2.2.2] octane). Typical experiments were carried out using the automated QCM instrument Q-Sense E4 Auto at 40 °C and at a flow rate of 100 µL/min. Each experiment started with exposing the PPMT functionalized QCM substrates first to the copper(II) acetate solution for 5 min and then equimolar mixture of linker bdc/dabco for 10 min. Each subsequent step of dosing components was separated by a washing step of 5 min with pure ethanol (in situ control by QCM for stable base line again). Alternatively, exposing the PPMT functionalized gold wafer firstly to the Cu(II) acetate solution for 15 min and then dosing a mixture of linker bdc/dabco for 30 min. Each subsequent step of dosing components was separated by a washing step with pure ethanol as described above. SURMOFs of $[Cu_2(NH_2\text{-}bdc)_2(dabco)]$ (**B**) and $[Cu_2(ndc)_2(dabco)]$ (**C**) can be prepared through the same procedures using NH_2-bdc or ndc instead of bdc. (NH_2-bdc = 2-amino-1,4-benzenedicarboxylate; ndc = 1,4-naphtalenedicarboxylate).

Preparation of Hybrid SURMOFs A-B and A-B-C: A: $[Cu_2(bdc)_2(dabco)]$ (m cycles), B: $[Cu_2(NH_2\text{-}bdc)_2(dabco)]$ (k cycles), C: $[Cu_2(ndc)_2(dabco)]$ (n cycles) ($10 \leq m, k, n \geq 30$). Typically, m = 15 cycles of **A** was fabricated on PPMT SAM on gold substrate (see above) and then k = 15 cycles of **B** was grown on top of previous 15 cycles of $[Cu_2(bdc)_2(dabco)]$ with same parameters and procedures except using NH_2-bdc instead of bdc, giving rise to the formation of h-SURMOF **A-B**. Another n = 15 cycles of **C** was grown on top of **B** on **A**, leading to the h-SURMOF **A-B-C**.

FPI Adsorption and Desorption Experiments: Prior to the FPI (4-fluorophenyl isothiocyanate m. p., 2 5°C) adsorption, SURMOF samples on gold substrate are evacuated by vacuum (<1 mbar) overnight at room temperature to remove accommodated ethanol (as checked by IR spectroscopy). Evacuated samples are exposed to the atmosphere of FPI at its naturally generated pressure overnight. FPI desorption was performed by evacuating loaded samples in vacuum overnight at room temperature. Samples **A**, **A-B** and **A-B-C** (15 cycles for each sub-multilayer of **A**, **B** and **C**) fabricated on PPMT SAM on QCM gold substrate were applied. The respective SURMOF sample was treated by vacuum to remove the ethanol molecules (solvent) hosted in as deposited SURMOFs. Before switching to vessel containing FPI, pure nitrogen gas (carrier gas) was flown over SURMOF sample to obtain stable baseline. The adsorption curve was recorded by QCM. The adsorption experiments are performed at a flow rate of 5 sccm of carrier gas of controlled by a flow meter and room temperature. The FPI vaporizing unit is set to 25 °C with a vapor pressure of FPI of 0.122 Torr. The relative humidity is 100% in comparison with the adsorption isotherms measured by BELQCM, which approximately refers to the last data point of the isotherms shown in SI.

Characterization: The SURMOF samples were characterized with infrared reflection absorption spectroscopy (IRRAS) and X-ray diffraction (XRD). IRRAS data were recorded using a Biorad Excalibur FTIR spectrometer (FTS 3000) with 2 cm^{-1} resolution at an angle of incidence of 80° relative to the surface normal and further processed by using boxcar apodization. The X-ray diffraction experiments were carried out on Bruker AXS. The out-of-plane measurements were performed on a D8 Advance Diffractometer with kα Cu-radiation (Cu-Kα = 0.15418 nm) in the θ-2θ geometry and with a position sensitive detector. The measurements were carried out over a 2 theta range of 5–20 ° with a step size of 0.01° and a scan time of 1 s. The in-plane measurements were performed using a D8 Discover Diffractometer (Cu-Kα = 0.15418 nm) which is equipped with a quarter-Euler cradle. After sample position correction, a 2θ-ω scan in the range of 5–20 ° with a 0.02 ° step size and a scan time of 2 s was performed to collected data. Both diffractometers were equipped with a LynxEye Si-strip detector, which reduces measurement times in the best case to a point detector by a factor of approximately 200. SEM images were taken on a LEO1530 Gemini FESEM. An automated QCM instrument Q-Sense E4 Auto was used to monitor the SURMOF growth and FPI adsorption. The X-ray photoelectron spectroscopy (XPS) measurements were performed in a UHV apparatus ($<3 \times 10^{-10}$ mbar) based on a modified Leybold XPS system with a double-anode X-ray source.

Supporting Information

Supporting Information is available from the Wiley Online Library or from the author.

Acknowledgements

This work was funded within the priority program of the German Research Foundation (DFG) on metal–organic Frameworks (SPP 1362). B.L. is grateful for a stipend from the Alexander von Humboldt Foundation. M.T. is grateful for a PhD fellowship donated by the China Scholarship Council (CSC). Dr. Peter G. Weidler is thanked for his helpful discussion on XRD.

Received: October 15, 2012
Revised: December 10, 2012
Published online: March 1, 2013

[1] a) For a selection of current reviews, see the themed issue on *Metal Organic Frameworks* (Ed: J. Long, O. M. Yaghi), *Chem. Soc. Rev.* **2009**, *38*, 1203; b) B. Chen, C. Liang, J. Yang, D. S. Contreras, Y. L. Clancy, E. B. Lobkovsky, O. M. Yaghi, S. Dai, *Angew. Chem. Int. Ed.* **2006**, *45*, 1390; c) B. Chen, S. Xiang, G. Qian, *Acc. Chem. Res* **2010**, *43*, 1115.

[2] a) S. Kitagawa, R. Kitaura, S. Noro, *Angew. Chem. Int. Ed.* **2004**, *43*, 2334; b) G. Férey, *Chem. Soc. Rev.* **2008**, *37*, 191; c) H-L. Jiang, Q. Xu, *Chem. Commun.* **2011**, *47*, 3351.

[3] Z. Wang, S. M. Cohen, *Chem. Soc. Rev.* **2009**, *38*, 1315.

[4] M. Eddaoudi, J. Kim, N. Rosi, D. Vodak, J. Wachter, M. O'Keeffe, O. M. Yaghi, *Science* **2002**, *295*, 469.

[5] a) X. C. Huang, Y. Y. Lin, J.–P. Zhang, X. M. Chen, *Angew. Chem. Int. Ed.* **2006**, *45*, 1557; b) K. S. Park, Z. Ni, A. P. Côté, J. Y. Choi, R. Huang, F. J. Uribe-Romo, H. K. Chae, M. O'Keefe, O. M. Yaghi, *Proc. Natl. Acad. Sci. USA* **2006**, *103*, 10186.

[6] a) D. N. Dybtsev, H. Chun, K. Kim, *Angew. Chem. Int. Ed.* **2004**, *43*, 5033; b) K. Koh, A. G. Wong-Foy, A. J. Matzger, *Angew. Chem. Int. Ed.* **2008**, *47*, 677; c) T. Gadzikwa, O. K. Farha, C. D. Malliakas, M. G. Kanatzidis, J. T. Hupp, S. T. Nguyen, *J. Am. Chem. Soc.* **2009**, *131*, 13613.

[7] a) H. Chun, D. N. Dybtsev, H. Kim, K. Kim, *Chem. Eur. J.* **2005**, *11*, 3521; b) D. Tanaka, M. Higuchi, K. Hasegawa, S. Horike, R. Matsuda, Y. Kinoshita, N. Yanai, S. Kitagawa, *Chem. Asian J.* **2008**, *3*, 1343; c) T. Uemura, Y. Ono, K. Kitagawa, S. Kitagawa, *Macromolecules* **2008**, *41*, 87; d) H. Wang, J. Getzschmann, I. Senkovska, S. Kaskel, *Microporous Mesoporous Mater.* **2008**, *116*, 653; e) P. Song,

Y. Li, B. He, J. Yang, J. Zheng, X. Li, *Microporous Mesoporous Mater.* **2008**, *142*, 208.
[8] D. Bradshaw, J. B. Claridge, E. J. Cussen, T. J. Prior, M. J. Rosseinsky, *Acc. Chem. Res.* **2005**, *38*, 273.
[9] a) D. Bradshaw, T. J. Prior, J. Cussen, J. B. Claridge, M. J. Rosseinsky, *J. Am. Chem. Soc.* **2004**, *126*, 6106; b) D. N. Dybtsev, A. L. Nuzhdin, H. Chun, K. P. Bryliakov, E. P. Talsi, V. P. Fedin, K. Kim, *Angew. Chem. Int. Ed.* **2006**, *45*, 916.
[10] S. S.-Y. Chui, S. M. F. Lo, J. P. H. Charmant, A. G. Orpen, I. D. Williams, *Science* **1999**, *283*, 1148.
[11] a) G. Férey, C. Mellot-Draznieks, C. Serre, F. Millange, J. Dutour, S. Surble, I. Margiolaki, *Science* **2005**, *309*, 2040; b) C. Serre, F. Millange, C. Thouvenot, M. Nogues, G. Marsolier, D. Loüer, G. Férey, *J. Am. Chem. Soc.* **2002**, *124*, 13519; c) T. Loiseau, C. Serre, C. Huguenard, G. Fink, F. Taulelle, M. Henry, T. Bataille, G. Férey, *Chem. Eur. J.* **2004**, *10*, 1.
[12] a) A. D. Burrows, *Cryst Eng Comm.* **2011**, *13*, 3623; b) W. Kleist, F. Jutz, M. Maciejewski, A. Baiker, *Eur. J. Inorg. Chem.* **2009**, *44*, 3552; c) H. Deng, C. Doonan, J. Furukawa, H. Ferreira, R. B. Towne, J. C. B. Knobler, B. Wang, O. M. Yaghi, *Science* **2010**, *327*, 843; d) A. D. Burrows, C. G. Frost, M. F. Mahon, C. Richardson, *Angew. Chem. Int. Ed.* **2008**, *47*, 8482; e) S. Marx, W. Kleist, J. Huang, M. Maciejewski, A. Baiker, *Dalton Trans.* **2010**, *39*, 3795; f) K. M. L. Taylor-Pashow, J. D. Rocca, Z. Xie, S. Tran, W. Lin, *J. Am. Chem. Soc.* **2009**, *131*, 14261; g) T. Fukushima, S. Horike, Y. Inubushi, K. Nakagawa, Y. Kubota, M. Takata, S. Kitagawa, *Angew. Chem. Int. Ed.* **2010**, *49*, 4820; h) W. Kleist, M. Maciejewski, A. Baiker, *Thermochim. Acta* **2010**, *499*, 71; i) A. D. Burrows, L. C. Fisher, C. Richardson, S. P. Rigby, *Chem. Commun.* **2011**, *47*, 3380.
[13] S. Furukawa, K. Hirai, Y. Takashima, K. Nakagawa, M. Kondo, T. Tsuruoka, O. Sakata, S. Kitagawa, *Chem. Commun.* **2009**, 5097.
[14] a) S. Furukawa, K. Hirai, K. Nakagawa, Y. Takashima, R. Matsuda, T. Tsuruoka, M. Kondo, R. Haruki, D. Tanaka, H. Sakamoto, S. Shimomura, O. Sakata, S. Kitagawa, *Angew. Chem. Int. Ed.* **2009**, *48*, 1766; b) Y.-S. Yoo, H.-K. Jeong, *Cryst. Growth Des.* **2010**, *10*, 1283; c) K. Koh, A. G. Wong-Foy, A. Matzger, *J. Chem. Commun.* **2009**, 6162.
[15] a) G. Demazeau, *J. Mater. Sci.* **2008**, *43*, 2104; b) R. I. Walton, F. Millange, R. L. Smith, T. C. Hansen, D. O'Hare, *J. Am. Chem. Soc.* **2001**, *123*, 12547.
[16] a) O. Shekhah, H. Wang, D. Zacher, R.A. Fischer, C. Wöll, *Angew Chem. Int. Ed.* **2009**, *48*, 5038; b) D. Zacher, R. Schmid, C. Wöll, R. A. Fischer, *Angew. Chem. Int. Ed.* **2011**, *50*, 176; c) B. Liu, R. A. Fischer, *Sci. China Chem.* **2011**, *54*, 1851; d) R. Makiura, S. Motoyama, Y. Umemura, H. Yamanaka, O. Sakata, H. Kitagawa, *Nat. Mater.* **2010**, *9*, 565.
[17] C. Munuera, O. Shekhah, H. Wang, C. Wöll, C. Ocal, *Phys. Chem. Chem. Phys.* **2008**, *10*, 7257.
[18] a) O. Shekhah, K. Hirai, H. Wang, H. Uehara, M. Kondo, S. Diring, D. Zacher, R. A. Fischer, O. Sakata, S. Kitagawa, S. Furukawa, C. Wöll, *Dalton Trans.* **2011**, *40*, 4954; b) D. Zacher, K. Yusenko, A. Bétard, K. Henke, M. Molon, L. Ladnorg, O. Shekhah, B. Schüpbach, T. de los Arcos, M. Meilikhov, A. Terfort, C. Wöll, R. A. Fischer, *Chem. Eur. J.* **2011**, *17*, 1448.
[19] O. Shekhah, H. Wang, M. Paradinas, C. Ocal, B. Schüpbach, A. Terfort, D. Zacher, R. A. Fischer, C. Wöll, *Nat. Mater.* **2009**, *8*, 481.
[20] B. Liu, M. Ma, D. Zacher, A. Báetard, K. Yusenko, N. Metzler-Nolte, C. Wöll, R. A. Fischer, *J. Am. Chem. Soc.* **2011**, *133*, 1734.
[21] a) M. L. Royer, *Bull. Soc. Fr. Mineral.* **1928**, *51*, 7; b) F. Ratto, F. Rosei, *Mater Sci. Eng., R* **2010**, *70*, 243.
[22] a) H. K. Jeong, J. Krohn, K. Sujaoti, M. Tsapatsis, *J. Am. Chem. Soc.* **2002**, *124*, 12966; b) T. Wakihara, S. Yamakita, K. Iezumi, T. Okubo, *J. Am. Chem. Soc.* **2003**, *125*, 12388.
[23] K. Yusenko, M. Meilikhov, D. Zacher, F. Wieland, C. Sternemann, X. Stammer, T. Ladnorg, C. Wöll, R. A. Fischer, *CrystEngComm.* **2010**, *12*, 2086.
[24] a) O. Shekhah, *Materials* **2010**, *3*, 1302; b) O. Shekhah, H. K. Arslan, K. Chen, M. Schmittel, R. Maul, W. Wenzele, C. Wöll, *Chem. Commun.* **2011**, *47*, 11210.
[25] a) H. Maeda, N. Ishida, H. Kawauchi, K. Tuzimura, *J. Biochem.* **1969**, *65*, 777; b) H. Salmio, D. Brühwiler, *J. Phys. Chem. C* **2007**, *111*, 923; c) H. Ritter, D. Brühwiler, *J. Phys. Chem. C* **2009**, *113*, 10667.
[26] M. Szaleniec, R. Tokarz-Sobieraj, W. Witko, *J. Mol. Model* **2009**, *15*, 935.
[27] O. Zybaylo, O. Shekhah, H. Wang, M. Tafipolsky, R. Schmid, D. Johannsmann, C. Wöll, *Phys. Chem. Chem. Phys.* **2010**, *12*, 8092.
[28] B. Liu, O. Shekhah, H. K. Arslan, J. Liu, C. Wöll, R. A. Fischer, *Angew. Chem. Int. Ed.* **2011**, *51*, 807.
[29] a) Y. Liu, W. Zhang, S. Xie, L. Xu, X. Han, X. Bao, *J. Phys. Chem. B* **2008**, *112*, 1226; b) Y. Liu, W. Zhang, Z. Liu, S. Xu, Y. Wang, Z. Xie, X. Han, X. Bao, *J. Phys. Chem. C* **2008**, *112*, 15375; c) K. J. Ooms, R. E. Wasylishen, *Microporous Mesoporous Mater.* **2007**, *103*, 341.
[30] A. S. Münch, J. Seidel, A. Obst, E. Weber, F. O. R. L. Mertens, *Chem. Eur. J.* **2011**, *17*, 10958.
[31] A. Bétard, H. Bux, S. Henke, D. Zacher, J. Caro, R. A. Fischer, *Microporous Mesoporous Mater.* **2012**, *150*, 76.